NF-M is an essential target for the myelin-directed "outside-in" signaling cascade that mediates radial axonal growth

Michael L. Garcia,[1,2,3] Christian S. Lobsiger,[1,2] Sameer B. Shah,[2,6] Tom J. Deerinck,[4] John Crum,[4] Darren Young,[1] Christopher M. Ward,[1,2] Thomas O. Crawford,[7] Takahiro Gotow,[8] Yasuo Uchiyama,[9] Mark H. Ellisman,[4] Nigel A. Calcutt,[5] and Don W. Cleveland[1,2,3]

[1]Ludwig Institute for Cancer Research, [2]Department of Cellular and Molecular Medicine, [3]Department of Neuroscience, [4]National Center for Microscopy and Imaging Research, and [5]Department of Pathology, [6]Howard Hughes Medical Institute, University of California at San Diego, La Jolla, CA 92093
[7]Department of Neurology, Johns Hopkins University School of Medicine, Baltimore, MD 21205
[8]Laboratory of Cell Biology, College of Nutrition, Koshien University, Hyogo 665-0006, Japan
[9]Department of Cell Biology and Neurosciences, Osaka University Graduate School of Medicine, Osaka 565-0871, Japan

Neurofilaments are essential for acquisition of normal axonal calibers. Several lines of evidence have suggested that neurofilament-dependent structuring of axoplasm arises through an "outside-in" signaling cascade originating from myelinating cells. Implicated as targets in this cascade are the highly phosphorylated KSP domains of neurofilament subunits NF-H and NF-M. These are nearly stoichiometrically phosphorylated in myelinated internodes where radial axonal growth takes place, but not in the smaller, unmyelinated nodes. Gene replacement has now been used to produce mice expressing normal levels of the three neurofilament subunits, but which are deleted in the known phosphorylation sites within either NF-M or within both NF-M and NF-H. This has revealed that the tail domain of NF-M, with seven KSP motifs, is an essential target for the myelination-dependent outside-in signaling cascade that determines axonal caliber and conduction velocity of motor axons.

Introduction

It has long been known that myelination (de Waegh et al., 1992) is essential for specification of growth in axonal volume of the largest motor and sensory axons after stable synapse formation. The initial signaling steps in this "outside-in" signaling cascade have been identified. During myelination, which in rodents is completed by 4 wk postnatally (Mirsky et al., 2002), myelin-associated glycoprotein (MAG) is redistributed to membrane domains juxtaposed to axonal regions, timing that is consistent with the initial wave of radial growth (Bartsch et al., 1989; Trapp et al., 1989). The probable axonal MAG receptor responsible for transducing the myelin signal into axons is the low affinity nerve growth factor receptor, p75[NTR] (Wang et al., 2002; Wong et al., 2002; Yamashita et al., 2002), most likely in association with neuronal gangliosides

GT1b and GD1a (Yang et al., 1996a; Vyas et al., 2002). Upon activation of p75[NTR], three type II MAGE family members (NRAGE, necdin, and MAGEH-1) are known to interact with p75[NTR] (Salehi et al., 2000; Tcherpakov et al., 2002), forming a cytoplasmic surface for recruitment of signal transducing molecules including upstream activators of extracellular signal–regulated protein kinase 1/2 (ERK1/2).

Despite these insights, the target(s) for such a kinase cascade has not been established. Analysis of neurofilament expression after axonal recovery from crush injury initially suggested a role for neurofilaments in establishing axonal diameter (Hoffman et al., 1987). Obligate heteropolymers of neurofilament light (NF-L), medium (NF-M), and heavy (NF-H) neurofilaments are the most abundant structural component of large myelinated axons. As with most neuronal proteins, they are synthesized in the neuronal soma and
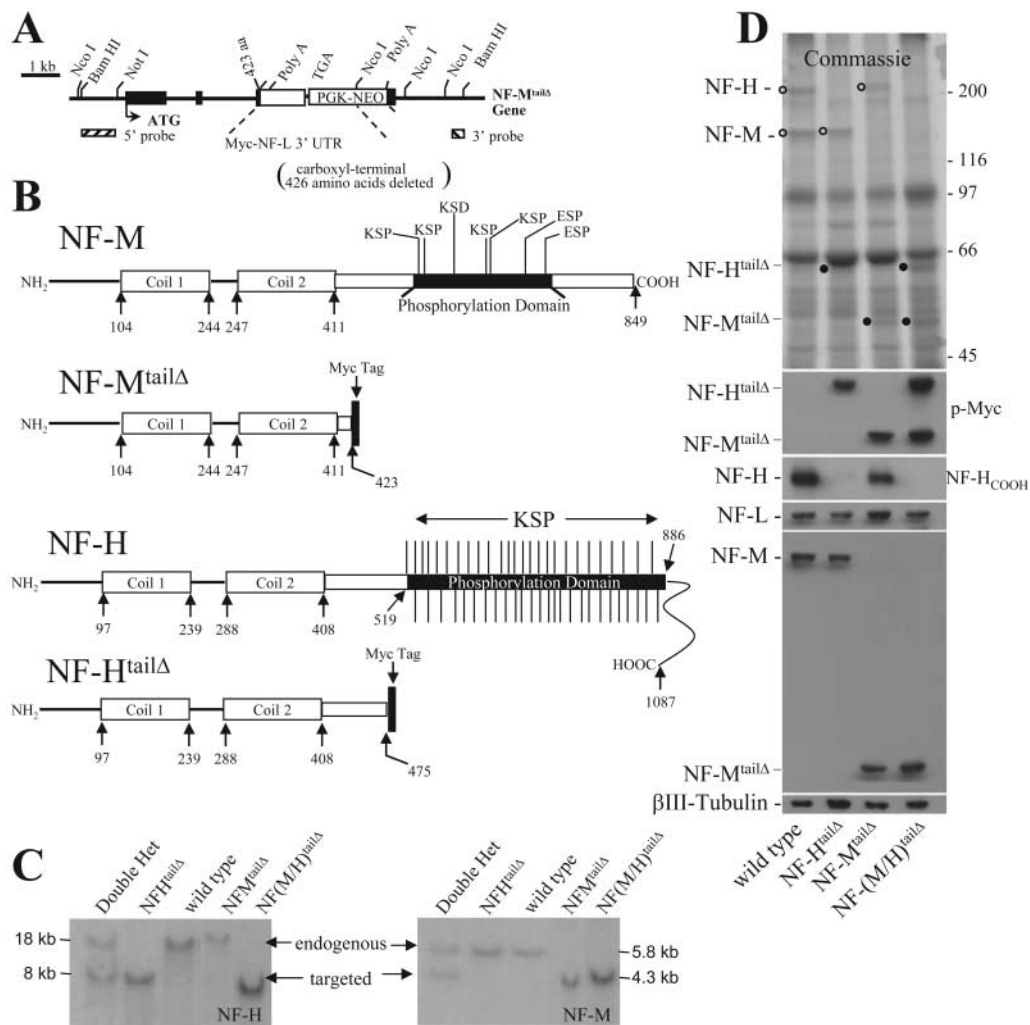
Figure 1. **Substitution of NF-M[tailΔ] for wild-type NF-M does not affect stoichiometry of the neurofilament subunits.** (A) Schematic of targeted NF-M gene in which 426 amino acids of the tail domain are replaced with a 12–amino acid c-myc epitope tag. The three exons of the NF-M gene are indicated by the filled boxes interrupted by three introns. ATG denotes the translation initiation codon. (B) Representation of NF-M[tailΔ] and NF-H[tailΔ] proteins generated by gene replacement of both endogenous NF-M and NF-H genes. (C) Mouse genomic DNA was screened for targeted truncation of NF-M and NF-H tails. (Left) Genotyping the NF-H loci by hybridizing with a sequence from NF-H (Rao et al., 2002). (Right) Genotyping the NF-M loci by hybridization to the sequence in A marked "5′ probe." (D) Loss of NF-M, NF-H, or both tails has no effect on relative stoichiometries and accumulated levels of NF-L, NF-M, NF-H, or tubulin. Parallel immunoblots of sciatic nerve extracts from each of three sets of 2- and 6-mo-old wild-type, NF-H[tailΔ], NF-M[tailΔ], and NF-(M/H)[tailΔ] homozygous mice were fractionated on 7.5% SDS-polyacrylamide gels and stained with (top) Coomassie blue or immunoblotted with antibodies that recognize NF-H in a phospho-independent manner (pAb-NF-H[COOH]), an epitope in the helical rod of NF-M (RMO-44), the epitope tag on NF-H[tailΔ] or NF-M[tailΔ], NF-L, or the neuron-specific β[III]-tubulin (MLR11).

are subsequently transported into the axon via slow axonal transport. Once in the axon, neurofilaments are extremely long-lived proteins involved in establishing and maintaining the three-dimensional array of axoplasm.

Genetics in both mouse and quail unequivocally confirmed that neurofilaments are required for determining mature axonal diameter in myelinated regions. In mouse, loss of neurofilaments (Ohara et al., 1993; Eyer and Peterson, 1994; Elder et al., 1998; Jacomy et al., 1999; Zhu et al., 1997) markedly suppresses the many fold growth in axonal diameter (and volume) that initiates during myelination. Moreover, axonal diameter is sensitive to the subunit composition, as increased expression of any single neurofilament subunit inhibits radial growth (Monteiro et al., 1990; Cote et al., 1993; Collard et al., 1995; Tu et al., 1995; Wong et al., 1995; Marszalek

et al., 1996; Xu et al., 1996), whereas simultaneous overexpression of NF-L and NF-M or NF-H increases overall axonal diameter (Xu et al., 1996). Expression of full-length neurofilament subunits and various truncation mutations in nonneuronal cells resulted in 10-nm fibers that formed COOH-terminal, phosphorylated cross-bridges that extended along the length of the filament (Nakagawa et al., 1995; Chen et al., 2000). In sciatic nerve, these COOH-terminal cross-bridges seem to span between adjacent neurofilaments and between neurofilaments and microtubules (Hirokawa et al., 1984; Rao et al., 2002). Thus, neurofilament-dependent structuring of axoplasm is likely to be mediated, at least in part, by these extended COOH-terminal tails of NF-M and NF-H.

Neurofilament-dependent radial growth is itself associated with phosphorylation of the COOH-terminal tail domains
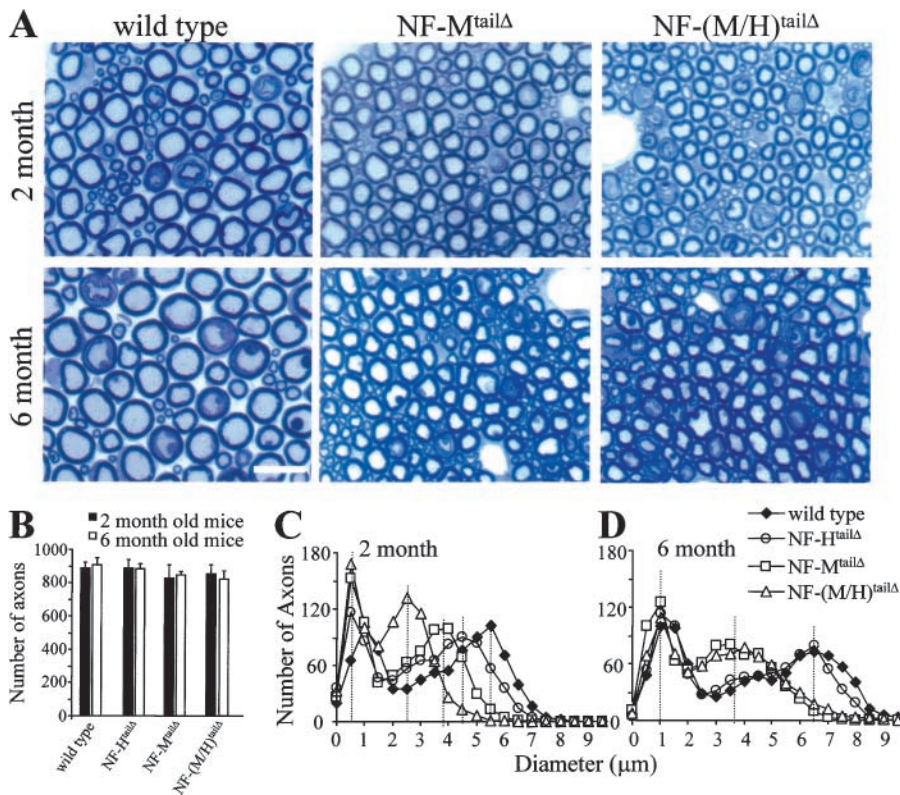
Figure 2. **Absence of NF-M or both NF-M and NF-H tail domains reduces radial growth of motor axons but does not markedly affect their survival.** (A) Cross sections of L5 motor (ventral root) axonal profiles from wild-type, NF-M$^{tail\Delta}$, and NF-(M/H)$^{tail\Delta}$ homozygous mice at (top) 2 mo or (bottom) 6 mo of age. Bar, 10 μm. Numbers of axons in L5 motor roots of 2- or 6-mo-old wild-type and NF-M$^{tail\Delta}$ and NF-(M/H)$^{tail\Delta}$ homozygous mice (B). Counts are average from four to five animals for each genotype. (C and D) Distributions of axonal diameters in motor axons in (C) 2- or (D) 6-mo-old wild-type, NF-H$^{tail\Delta}$, NF-M$^{tail\Delta}$, and NF-(M/H)$^{tail\Delta}$ homozygous animals. Points represent the averaged distribution of axon diameters form the entire roots of five mice for each genotype and age group.

of both NF-M and NF-H, which in mice contain 7 and 51 KSP phosphorylation motifs, respectively. While neurofilaments are required for proper post-natal growth of axons, several lines of evidence suggest that neurofilament phosphorylation is essential for proper axonal diameter and that phosphorylation is regulated by myelinating cells (de Waegh et al., 1992; Yin et al., 1998). The KSP motifs of both NF-M and NF-H are nearly stoichiometrically phosphorylated (Julien and Mushynski, 1982) in the myelinated segments that undergo radial growth, whereas they are unphosphorylated in the narrow unmyelinated initial segment and the nodes of Ranvier (Hsieh et al., 1994). Further, axonal segments ensheathed by myelin-defective Schwann cells do not undergo post-natal growth, whereas segments of the same axons ensheathed by myelin-competent Schwann cells achieve large axonal diameters (de Waegh et al., 1992).

This has raised the possibility that the outside-in signal cascade originating from myelinating cells functions to activate axonal kinases (or inactivates phosphatases or both) that act directly on neurofilaments. We now use replacement of the NF-M and NF-H genes in mice to test this model of a myelination-dependent phosphorylation cascade targeting the tail domains of NF-M and NF-H as an essential feature of radial axonal growth.

Results

Stoichiometric substitution of NF-M and NF-H with NF-M and NF-H subunits deleted in KSP phosphorylation motifs

Mice carrying an NF-M gene in which the 426 COOH-terminal tail amino acids (NF-M$^{tail\Delta}$) containing seven KSP mo-

tifs was replaced by a 12–amino acid Myc epitope tag (Fig. 1, A and B) were generated and bred to similar mice (NF-H$^{tail\Delta}$) in which the NF-H tail, including its 51 KSP phosphorylation sites, was replaced with the same Myc epitope tag (Rao et al., 2002) (Fig. 1 B). Mice heterozygous for both COOH terminally truncated neurofilaments were then interbred to produce, within the same litters, animals that were homozygous for either or both (the latter to be referred to as NF-[M/H]$^{tail\Delta}$), as well as wild-type controls (Fig. 1 C). All genotypes were produced at expected Mendelian frequencies with no overt phenotype at the oldest ages analyzed (1.5 yr).

Coomassie blue staining of sciatic nerve extracts revealed the loss of both full-length NF-M and NF-H in NF-M$^{tail\Delta}$ and NF-H$^{tail\Delta}$ animals and the appearance of new 50- and 62-kD polypeptides corresponding to NF-M and NF-H subunits, respectively, that were missing their known phosphorylation sites (Fig. 1 D). When corrected for the differences in mass and assuming Coomassie dye binding to be independent of polypeptide sequence, densitometry of such gels revealed that in nerves from animals homozygous for either or both NF-M$^{tail\Delta}$ and NF-H$^{tail\Delta}$ polypeptides, the molar levels of each of the three neurofilament subunits were indistinguishable from that of the corresponding full-length subunits in wild-type animals (Fig. 1 D). Immunoblotting using an antibody that recognizes an epitope within the helical rod domain of murine NF-M (RMO44; Fig. 1 D) yielded equivalent signal intensities as NF-M in normal nerves, confirming that NF-M$^{tail\Delta}$ accumulated to the normal NF-M level. Furthermore, the level of accumulated NF-M$^{tail\Delta}$ was independent of whether NF-H was full length or truncated. Similarly, NF-L levels, as well as the neuron-specific β-III tubulin, were constant regardless of the genotype at the NF-M or NF-H loci. When taken to-

Figure 3. **Structure of axoplasm in the presence or absence of NF-M and NF-H tail domains.** (A–C) Transmission electron micrographs of 2-mo-old motor axons derived from the fifth lumbar spinal cord segment of (A) wild-type, (B) NF-M$^{tail\Delta}$, and (C) NF-(M/H)$^{tail\Delta}$ mice. Bar, 200 nm. Distribution of nearest neighbor distances from motor axons of (D) 2- and (E) 6-mo-old wild-type, NF-M$^{tail\Delta}$, and NF-(M/H)$^{tail\Delta}$ mice. (F–H) Quick-freeze, deep-etch micrographs of sciatic nerves from (F) wild-type, (G) NF-M$^{tail\Delta}$, and (H) NF-(M/H)$^{tail\Delta}$ mice. Bar, 100 nm. Arrowheads point to cross-linkers projecting from the core of neurofilaments. Arrows point to plectin-like linkers.
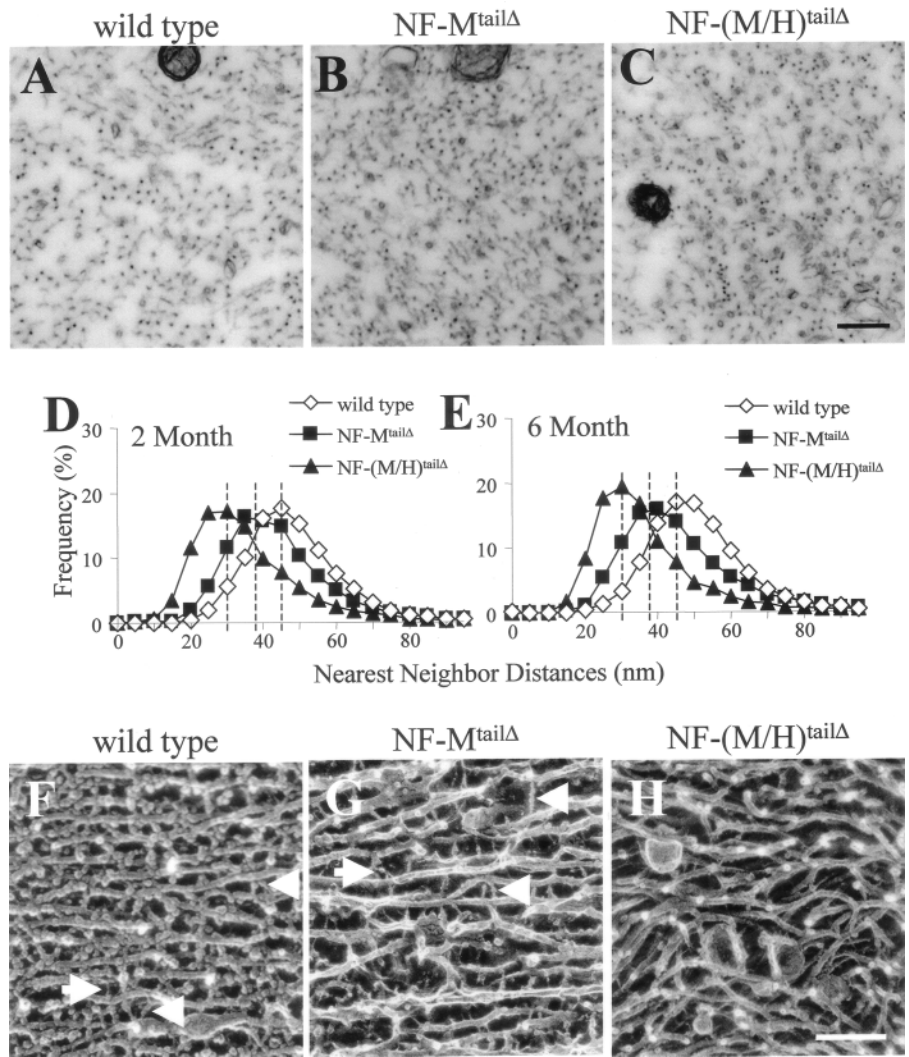
gether with our earlier demonstration that NF-H$^{tail\Delta}$ subunits accumulate to the normal NF-H level in NF-H$^{tail\Delta}$ nerves (Rao et al., 2002), the neurofilament subunit numbers and ratios are equivalent in the mice with or without either or both of the NF-M or NF-H KSP phosphorylation sites.

NF-M tail and its phosphorylations are essential for radial growth of large myelinated motor axons

To determine how loss of the NF-M tail and its myelination-dependent phosphorylation sites affected radial axonal growth and survival, sizes of all axons from the fifth lumbar vertebra were determined at 2 mo, an age just after the initial burst of radial growth in mice with wild-type neurofilament content. Cross-sectional areas were measured for all axons, and equivalent diameters were calculated. Replacement of the NF-M or NF-H tails or both had no effect on the initial number of motor axons at 2 mo of age (Fig. 2 B) or on their survival to 6 mo (Fig. 2 B). While wild-type and NF-M$^{tail\Delta}$ ventral root axons yielded bimodal distributions of axonal sizes, both the larger (>2 μm) and smaller (<2 μm) classes of myelinated fibers of NF-M$^{tail\Delta}$ axons failed to achieve diameters comparable to that seen in wild-type animals (Fig. 2 A).

Moreover, unlike wild-type axons that continue radial growth through 6 mo of age (Fig. 2 A), large myelinated fibers from NF-M$^{tail\Delta}$ failed to grow in this subsequent 4 mo period (compare squares, Fig. 2, C and D). Relative to NF-M$^{tail\Delta}$ axons, simultaneous loss of the NF-H tail and its 51 KSP phosphorylation sites in the NF-(M/H)$^{tail\Delta}$ animals affected the speed with which radial growth was achieved and the final size relative to controls. Axonal cross-sectional areas >2 μm in diameter in NF-(M/H)$^{tail\Delta}$ animals were half that of NF-M$^{tail\Delta}$ axons at 2 mo (Fig. 2 C), but by 6 mo, NF-(M/H)$^{tail\Delta}$ axons achieved axonal size distributions indistinguishable from NF-M$^{tail\Delta}$ mice (Fig. 2 D). Analysis of axons from NF-H$^{tail\Delta}$ littermates confirmed the influence of the NF-H tail on the rate, but not the final magnitude, of axonal growth; at 2 mo, motor axons >2 μm in NF-H$^{tail\Delta}$ mice were on average 1.5 μm smaller than in axons with wild-type NF-H, but the distributions were indistinguishable by 6 mo (Fig. 2 D). Thus, the tail domain of NF-M, but not NF-H, is essential for establishing mature calibers of large myelinated motor axons.

Axonal organization but not myelination-dependent radial growth is linked to cross-bridging between adjacent neurofilaments

To determine how the tail of NF-M and its myelination-dependent phosphorylation affects axonal organization of neurofilaments and microtubules and how this relates to estab-
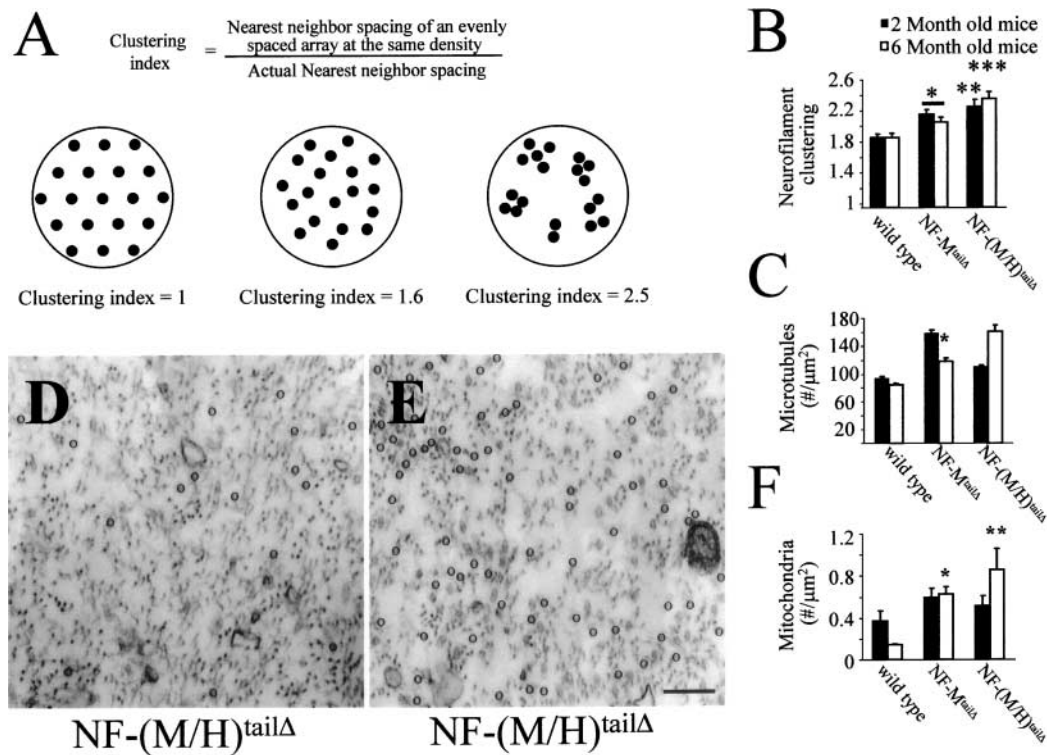
Figure 4. **Neurofilament tail domains are required for organizing axoplasm.** (A) Neurofilaments (black dots) in cross sections of ideal, wild-type, and NF-(M/H)$^{tail\Delta}$ axons were rearranged to form an array of regular hexagons encompassing the equivalent cross-sectional area. Note that the number of neurofilaments in all conditions is equal, however, the average distance each neurofilament is shifted to form triangle vertices is much greater for the tailless axon. (B) Neurofilament clustering, defined as the ratio of average filament spacing to nearest neighbor spacing, was significantly higher in both NF-M$^{tail\Delta}$ and NF-(M/H)$^{tail\Delta}$ mice at both 2 and 6 mo, indicating less axoplasmic organization in mice expressing truncated neurofilaments. Clustering was analyzed for overall statistical analysis using ANOVA with subsequent Tukey-Kramer multiple comparison post-hoc analysis for pairwise comparisons. *, $P < 0.05$ NF-M$^{tail\Delta}$ versus wild type at 2 and 6 mo; **, $P < 0.01$ NF-(M/H)$^{tail\Delta}$ versus wild type at 2 mo; ***, $P < 0.001$ NF-(M/H)$^{tail\Delta}$ versus wild type at 6 mo. (C–E) Microtubule content was reflective of overall axoplasmic disorganization. A trend toward accumulating more microtubules occurred in both NF-M$^{tail\Delta}$ and NF-(M/H)$^{tail\Delta}$ mice (C) but did not reach statistical significance. (D and E) Electron micrographs from two different axons of the same L5 motor root from a single NF-(M/H)$^{tail\Delta}$ mouse highlights the heterogeneity of microtubule accumulation that results from loss of both NF-M and NF-H tail domains. Bar, 200 nm. Microtubule content was analyzed for overall statistical significance using ANOVA with subsequent Bonferroni multiple comparison post-hoc analysis for pairwise comparisons. *, $P < 0.05$ NF-M$^{tail\Delta}$ versus wild type. (F) Mitochondria accumulate in regions of high axoplasmic disorganization. At 6 mo, in both NF-M$^{tail\Delta}$ and NF-(M/H)$^{tail\Delta}$ mice, vesicle accumulation was significantly higher than age-matched controls (F). Vesicle accumulation was analyzed for statistical significance using Mann-Whitney test. *, $P < 0.008$ NF-M$^{tail\Delta}$ versus wild type; **, $P < 0.05$ NF-(M/H)$^{tail\Delta}$ versus wild type.

lishment of axonal caliber, cross sections of motor axons were compared from wild-type, NF-M$^{tail\Delta}$, and NF-(M/H)$^{tail\Delta}$ mice (Fig. 3, A–C). Nearest neighbor spacing of neurofilaments was reduced (median values of 45–39 nm at 2 and 6 mo were estimated from approximate Gaussian distributions of neurofilament spacing) by loss of the NF-M tail compared with wild type at both 2 and 6 mo of age (Fig. 3, D and E). Thus, NF-M–dependent cross-bridging between adjacent neurofilaments is one determinant of nearest neighbor spacing. In the presence of the NF-M tail, nearest neighbor spacing is not influenced by the much more heavily phosphorylated NF-H tail, as deletion of the entire NF-H tail does not alter nearest neighbor spacing (Rao et al., 2002). However, the NF-H tail partially compensates for the loss of NF-M tail; at both 2 and 6 mo, deletion of both tail domains reduced average spacing even further (from median values of 45 to 30 nm at 2 and 6 mo) (Fig. 3, D and E).

Longitudinal views of axoplasm by quick-freeze, deep-etch microscopy revealed that in addition to the presence of some more closely spaced filaments, cross-bridges extending to or from the surface of neurofilaments (Fig. 3, F and G) were almost eliminated in the NF-(M/H)$^{tail\Delta}$, leaving smooth-walled filaments (Fig. 3 H), demonstrating that most of the in vivo cross-bridges between neurofilaments are provided by a combination of the phosphorylated tail domains of NF-M and NF-H. Additionally, despite the absence of the NF-M tail, and its influence on caliber, the neurofilaments remained aligned longitudinally, appearing qualitatively as straight as wild-type neurofilaments (Fig. 3 G). However, in the absence of both tail domains, the smooth-walled neurofilaments were much more curved, forming wavy, irregular arrays (Fig. 3 H).

In addition to altered nearest neighbor distances and neurofilament morphology, axoplasm was also less organized in the absence of both NF-M$^{tail\Delta}$ and NF-(M/H)$^{tail\Delta}$ mice. Axoplasm from both NF-M$^{tail\Delta}$ and NF-(M/H)$^{tail\Delta}$ mice contained subregions in which the axoplasm frequently appeared "unoccupied" as compared with the more even distribution in wild-type axoplasm (Fig. 3, compare A and C). This effect was quantified by analyzing neurofilament
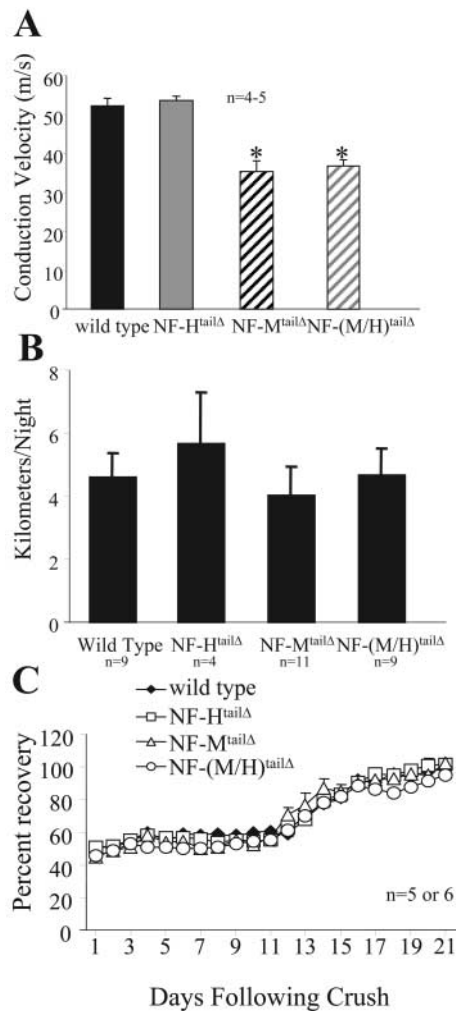
Figure 5. Absence of tail domains of NF-M or NF-M and NF-H slows nerve conduction velocity, but does not result in altered locomotor activity levels or recovery rates from sciatic nerve crush injury. (A) Nerve conduction velocity was measured from motor axons of the sciatic nerve from wild-type, NF-H$^{tail\Delta}$, NF-M$^{tail\Delta}$, and NF-(M/H)$^{tail\Delta}$ mice. Values shown are from a minimum of five animals for each genotype, and the recordings are done in triplicate for each animal. Conduction velocities were analyzed for overall statistical analysis using ANOVA with subsequent Bonferroni multiple comparison post-hoc analysis for pairwise comparisons. *, $P < 0.001$ for NF-M$^{tail\Delta}$ and NF-(M/H)$^{tail\Delta}$ versus both wild type and NF-H$^{tail\Delta}$. (B) Average daily activity levels were analyzed in wild-type, NF-H$^{tail\Delta}$, NF-M$^{tail\Delta}$, and NF-(M/H)$^{tail\Delta}$ mice. Mice were placed in activity chambers for a period of 14 d. Revolutions were stored on an activity wheel counter and then converted in kilometers based on a 5-inch diameter running wheel. A minimum of nine animals were analyzed for wild-type, NF-M$^{tail\Delta}$, and NF-(M/H)$^{tail\Delta}$ mice, and four NF-H$^{tail\Delta}$ mice were analyzed. (C) Functional recovery was measured in sciatic nerves that had been crushed at the level of the obturator tendon from wild-type, NF-H$^{tail\Delta}$, NF-M$^{tail\Delta}$, and NF-(M/H)$^{tail\Delta}$ mice. Values were plotted as a percentage of motor function before crush injury. A minimum of five mice per genotype were assayed, and measurements were performed in triplicate for each animal per day for 21 d after crush injury.

tios implying more clustered (less uniformly distributed) neurofilaments. Neurofilaments within each axon were redistributed into hexagonal arrays over a cross-sectional area equal to that of the axon (shown schematically in Fig. 4 A, left). Average neurofilament spacing was then defined to be the edge length of each hexagon. Using this measure, the array in wild-type mice diverged from the 1.0 value of a "perfectly ordered" array, yielding a clustering index of 1.8. After removal of either NF-M or both NF-M and NF-H tail domains (Fig. 4 B), neurofilaments in age-matched littermates were significantly more clustered, or less organized, with a clustering index of 2.5 in the NF-(M/H)$^{tail\Delta}$ mouse.

Microtubule content also reflected the axonal disorganization in the absence of both the NF-M and NF-H tails and their cross-bridges. An overall trend of increased microtubule content was seen, although this was not statistically significant in light of a high variability in microtubule content even in comparing axons of similar sizes within the same animals (Fig. 4 C). Indeed, unlike wild-type axons, individual NF-(M/H)$^{tail\Delta}$ axons displayed strikingly different microtubule contents (highlighted in two examples in Fig. 4, D and E). Moreover, axoplasmic disorganization due to loss of neurofilament tail domains resulted in an apparent increase in mitochondrial content, at least in proximal axonal segments of both NF-M$^{tail\Delta}$ and NF-(M/H)$^{tail\Delta}$ mice relative to control (Fig. 4 F).
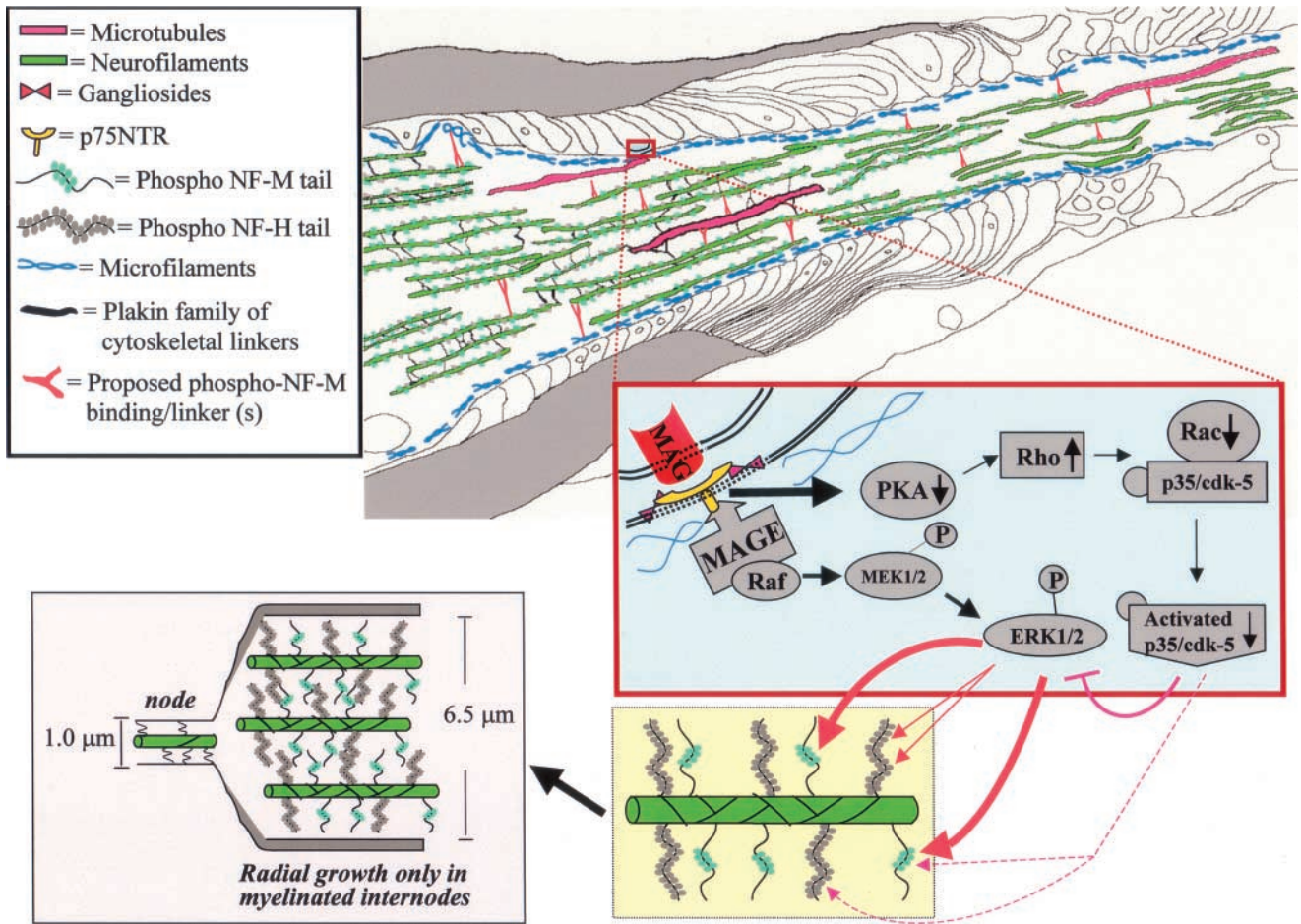
Slowed propagation of action potentials without NF-M tail–dependent expansion in axonal caliber

Motor axon conduction velocities were measured in the terminal segments of the sciatic nerves of 5–6-mo-old mice (five mice per genotype) from wild-type, NF-H$^{tail\Delta}$, NF-M$^{tail\Delta}$, and NF-(M/H)$^{tail\Delta}$ mice (Fig. 5 A). Consistent with the loss in diameter along the distal half of the largest caliber myelinated fibers, conduction velocity of action potentials was reduced ~30% in both NF-M$^{tail\Delta}$ and NF-(M/H)$^{tail\Delta}$ mice (Fig. 5 A).

Reduction in axonal caliber and conduction velocity does not alter locomotor activity levels or alter recovery after injury

Despite failure to acquire correct caliber and consequent reduction in conduction velocity, no overt phenotype was observed in mice with any of the altered neurofilament genotypes. Mice were provided running wheels, and their total distances run per night were measured to determine overall activity levels in wild-type, NF-H$^{tail\Delta}$, NF-M$^{tail\Delta}$, or NF-(M/H)$^{tail\Delta}$ mice (Fig. 5 B). Mice expressing truncated neurofilament subunits displayed activity levels indistinguishable from wild-type mice (Fig. 5 B).

Neurofilament synthesis and investment into proximal axons is suppressed after recovery from nerve crush (Hoffman et al., 1987), returning to normal levels only after recovery is complete. To determine if absence of major targets for the signaling cascade from myelinating cells to axons affects axonal recovery and regrowth after injury, sciatic nerves, at the level of the obturator tendon, were injured by crush, and the speed of recovery was assessed in NF-H$^{tail\Delta}$, NF-M$^{tail\Delta}$, NF-(M/H)$^{tail\Delta}$, and wild-type mice by measuring the spreading

clustering in both NF-M$^{tail\Delta}$ and NF-(M/H)$^{tail\Delta}$ mice versus age-matched wild-type littermates (Fig. 4, A and B). Neurofilament clustering was defined as the ratio of average filament spacing to nearest neighbor distance, with higher ra-

Figure 6. Model of myelin-dependent outside-in signaling cascade that controls radial axonal growth. In normal axons, axoplasmic organization is dependent upon myelinating cells. Signal cascades (Blue Box) originating from MAG in the membrane of myelinating cells utilize the low affinity nerve growth factor receptor (p75^{NTR}) in combination with neuronal gangliosides to transduce the myelin-dependent signal into the axoplasm. Upon association of MAG with p75^{NTR}, members of the melanoma antigen (MAGE) gene family associate with intracellular domain of p75^{NTR}, providing an intracellular scaffold for activation of ERK1/2 cascade, resulting in phosphorylation of NF-M (orange arrows) and NF-H (purple arrows) tail domains. MAG-dependent inactivation of p35/cdk-5 may reduce cdk-5 phosphorylation of NF-M and NF-H as well as prevent cdk-5–dependent inhibition of ERK1/2, allowing for near stoichiometric phosphorylation of NF-H and NF-M (yellow box). NF-M phosphorylation is required for establishing a volume-determining three-dimensional array (pink box) by a series of linkages that span between adjacent neurofilaments (green) and between neurofilament and microtubules (pink) or cortical actin (blue) filaments. Neurofilaments, microtubules, and cortical actin are interlinked by plakin family members of cytoskeletal linkers (blue) (Wiche, 1989; Eyer and Peterson, 1994; Svitkina et al., 1996). Axonal volume is, in part, established by a new class of linking protein that associates with neurofilaments in an NF-M tail phosphorylation–dependent manner to assist in long-range interactions that are necessary for the more than fivefold increase in axonal volume associated with radial growth.

distance between the first and fifth digit of the ipsilateral foot as a percentage of the spreading distance before injury. Recovery profiles from all genotypes were indistinguishable throughout 3 wk after injury (Fig. 5 C).

Discussion

We demonstrate that the tail of NF-M is an essential target for myelin-mediated axonal expansion. (Fig. 6). The simplest view is that the myelin-dependent signal cascade targets specific amino acids contained within the deleted region of NF-M tail as essential targets for phosphorylation through MAG-dependent signaling to the axon via p75^{NTR}-dependent activation of cyclin-dependent kinase 5 (cdk-5) and/or ERK1/2. Support for this model arises from many preceding efforts. Radial growth occurs only in myelinated regions of the axon

and is associated with increased neurofilament phosphorylation (de Waegh et al., 1992), including six of seven KSP repeat motifs within the NF-M tail (Xu et al., 1992). Neurofilament phosphorylation, interfilament spacing, and internodal axonal caliber are reduced in sciatic nerves of MAG-deficient mice (Yin et al., 1998), as they are in human neuropathies in which anti-MAG antibodies are present (Lunn et al., 2002). Similarly, loss of functional p75^{NTR}, either through antibody inhibition or through gene deletion, inhibits the accumulation of MAG and the formation of mature myelin internodes, and reduces the number of myelinated axons in adult sciatic nerve (Cosgaya et al., 2002). This is supported in vitro by direct binding of MAG-Fc chimeric proteins to PC12 cells; this yields an increase in NF-H and NF-M phosphorylation associated with increased activity levels of cdk-5 and ERK1/2 (Dashiell et al., 2002), both of

which have been shown in vitro to phosphorylate NF-H and NF-M, respectively (Pant et al., 1997; Veeranna et al., 1998).

It should be noted that despite strong inhibition of radial growth, some residual neurofilament phosphorylation remains in the absence of MAG (Yin et al., 1998). This probably reflects the recently recognized antagonistic roles of Rho and Rac in potentiating activation of cdk-5 and ERK1/2 (Niederost et al., 2002). MAG association with p75[NTR] activates Rho (Yamashita et al., 2002), possibly via a decrease in protein kinase A activity (Lehmann et al., 1999). Activated Rac, on the other hand, associates with cdk-5 and its activator p35, resulting in activation of cdk-5 kinase activity (Nikolic et al., 1998). Thus, in the absence of MAG, it is predicted that relative Rac activities are enhanced, yielding similarly enhanced cdk-5 kinase activity and cdk-5–dependent phosphorylation of both NF-M and NF-H. Moreover, additional kinases, such as Cdc-2–like kinase (Shetty et al., 1993) and cdk-5 activated by p67, its neuron-specific activator (Shetty et al., 1995), whose regulation may be independent of Rho and Rac, could be responsible for MAG-independent neurofilament phosphorylation within regions of the axon where MAG is known to localize. Taken together, the current evidence suggests that there are two distinct neurofilament phosphorylation events: (1) MAG dependent, resulting in radial growth, and (2) MAG independent, with little to no influence on radial growth.

The surprise in this mechanism underlying radial axonal growth is that it is interactions from the NF-M tail that are essential, rather than those of NF-H, which carries a much longer tail with many more sites (51 KSP sites in mice) that are nearly stoichiometrically phosphorylated. Truncation of NF-H by gene replacement in mice decreased the frequency of cross-bridges and increased the rate of radial growth, but did not alter the final caliber achieved (Rao et al., 2002). Thus, the myelin-derived signal results in an NF-H tail–dependent reduction in the rate, but not steady-state amount of axonal expansion.

As to how the NF-M tail mediates axonal growth in response to the myelin signal, it is clear that charge repulsion from neurofilament side arms does not play a key role. The much more heavily phosphorylated NF-H tail is neither necessary nor sufficient for neurofilament-dependent radial growth. Another simple model would be the assembly of a three-dimensional array of neurofilaments produced by nearest neighbor interactions that interlink the filaments into a space-filling, three-dimensional scaffold. This too cannot be completely correct because average interfilament spacing is altered in both NF-M[tailΔ] and NF-(M/H)[tailΔ] (Fig. 3, D and E) at both time points examined, yet at 6 mo, a time when NF-(M/H)[tailΔ] mice still have reduced interfilament distances relative to NF-M[tailΔ] mice, the calibers of NF-M[tailΔ] and NF-(M/H)[tailΔ] are indistinguishable (Fig. 2, C and D).

As the tail domains of NF-M and NF-H extend from the surface of the core filament, and site-specific phosphorylation apparently reduces the flexibility of this region (possibly due to local charge repulsion within the tail domain; Hisanaga and Hirokawa, 1988; Chen et al., 2000), the increased rigidity of phosphorylated neurofilament tail domains could serve two functions. First, semirigid neurofilament to neurofilament linkers, composed of NF-M and NF-H tail domains, could serve as hinge points allowing for a flexible cytoskeletal network that supports structure yet resists sudden alterations. Second, less flexible tail domains of either NF-M and/or NF-H mediate an increased spacing of adjacent neurofilaments. Increased interfilament distances may allow larger cytoskeletal linking proteins, including plectin (Wiche, 1998) and BPAG1n (Yang et al., 1996b), to associate efficiently with the neurofilament array. Increased rigidity or an increase in the number of nearest neighbor linkages stabilizes and straightens the core filament. Without these, as in the NF-(M/H)[tailΔ] mice, the neurofilament array is bowed, yielding overall axoplasmic disorganization.

Further, the almost complete loss of projections from NF-(M/H)[tailΔ] mice illustrates that nonneurofilament-derived cross-linking proteins, such as the plakin family of cytoskeletal linkers (Wiche, 1998), are relatively rare, or, more likely, efficient binding of these linkers to the neurofilament array requires that their binding sites be readily accessible through neurofilament tail domain–mediated increase in interfilament distances or that their binding sites are affected by the NF-M and NF-H tail domains and their phosphorylation. The NF-M tail domain and the myelin-dependent phosphorylation may position cytoskeletal linking proteins in a manner that facilitates longer-range interactions between neurofilaments and either actin filaments, tubulin, or both.

Materials and methods

Detection and quantification of neurofilament and tubulin proteins by immunoblotting

Sciatic and optic nerve extracts were made as previously described (Rao et al., 1998). Protein concentration was determined using bicinchoninic acid assay kit (Pierce Chemical Co.). Protein extracts, as well as known amounts of purified neurofilament standards, were separated on 7% polyacrylamide gels with SDS and transferred to nitrocellulose membranes (Lopata and Cleveland, 1987). The NF-H and NF-L subunits were identified using affinity-purified rabbit polyclonal antibodies pAb-NF-H[COOH] and pAb-NF-L[COOH] raised against the COOH-terminal 12 amino acids of mouse NF-H and NF-L, respectively (Xu et al., 1993). The epitope tag on the NF-M[tailΔ] and NF-H[tailΔ] subunit was detected with an affinity-purified polyclonal Myc antibody (Gill et al., 1990). mAbs to NF-M (RMO44; Tu et al., 1995) and neuron-specific, class III β-tubulin (MLR11; Lee et al., 1990) were used to identify each subunit, followed by goat anti–mouse IgG (Sigma-Aldrich) and ECL.

Tissue preparation, morphological analysis, and nearest neighbor analysis

Mice were perfused intracardially with 4% paraformaldehyde in 0.1 M Sorenson's phosphate buffer, pH 7.2, and postfixed overnight in the same buffer. Samples were treated with 2% osmium tetroxide, washed, dehydrated, and embedded in Epon-Araldite resin. Thick sections (0.75 μm) for light microscopy were stained with toluidine blue. Cross sections of L5 motor and sensory axons were analyzed in five to six mice per genotype and each age group. Axonal diameters were measured using the Bioquant Software. Entire roots were imaged, imaging thresholds were selected individually, and the cross-sectional area of each axon was calculated and reported as a diameter of a circle of equivalent area. Axon diameters were grouped into 0.5-μm bins.

Mice were prepared for conventional EM analysis by intracardial perfusion with Ringers solution followed by 2% glutaraldehyde and 2% formaldehyde in 0.15 M sodium cacodylate buffer, pH 7.4, at 35°C for 5 min. L5 motor and sensory roots were dissected, fixed on ice for 1–2 h, washed five times for 5 min in cold 0.15 M cacodylate buffer, postfixed in 1% OsO$_4$ in 0.15 M cacodylate buffer on ice for 1 h, and finally rinsed in cold double-distilled water five times for 5 min. After incubation with 1% uranyl acetate on ice for 16 h, roots were then rinsed in ice cold double distilled water three times for 3 min per rinse. Samples were dehydrated

through an ethanol series, embedded by initially infiltrating with 50% ethanol and 50% durcupan resin for 1 h at room temperature, and then changed to 100% resin for 1 h and placed into fresh resin for an additional hour. The resin was cured in a 60°C vacuum oven for 24–48 h. Samples were sectioned (60–80 nm), collected on grids, stained for 10 min in 1% aqueous uranyl acetate followed by 2 min staining with lead salts, and then alyzed on a JEOL 1200EX electron microscope at 60–80 kV.

Negatives were digitized with a 1024 × 1024 pixel CCD camera. Positions of individual neurofilaments were marked with an electronic pointer, and nearest neighbor distances were calculated using software written by Stephen Lamont (NCMIR; University of California, San Diego).

Methods for calculating neurofilament clustering
Average neurofilament spacing was determined by distributing identified neurofilaments in uniform arrays across the effective cross-sectional area of an axon. Cross-sectional area was estimated by tracing axoplasmic regions of the same digitized electron micrographs used to identify neurofilaments. Neurofilaments were organized in concentric hexagonal "rings" of equilateral triangles (Fig. 4 A), with average neurofilament spacing calculated as the side length of one triangle. Hexagons were selected due to their inherent ability to pack two-dimensional space optimally (Conway and Sloane, 1999). The number of counted neurofilaments (n_{NF}) corresponded to n_{tri} triangles, arranged into i hexagonal rings. The relationships between n_{NF}, n_{tri}, and I are given by the following recursive formulae:

$$n_{NF}(i) = n_{NF}(i-1) + 6*i$$

$$n_{tri}(i) = n_{tri}(i-1) + 6*[2*(i-1)+1],$$

with $n_{NF}(1) = 7$ and $n_{tri}(1) = 6$. Intermediate values (complete triangles within incomplete hexagonal rings) were calculated using interpolation. Average filament spacing was then calculated from the area of a single regular hexagon, which was determined by dividing the axonal cross-sectional area by n_{tri}. Neurofilament clustering was defined as the ratio of average filament spacing to nearest neighbor filament spacing, with higher ratios implying more clustered (less uniformly distributed) neurofilaments. Analysis was performed using MATLAB 6.5 (The MathWorks, Inc.).

Visualization of neurofilament organization in the axon by quick-freeze, deep-etch analysis
Sciatic nerves of 4–5-mo-old NF-M$^{tail\Delta}$ and their control littermate animals were dissected and incubated in oxygenated artificial cerebrospinal fluid containing (in mM, pH 7.3) 126 NaCl, 22 NaHCO$_3$, 1 Na$_2$HPO$_4$, 2.8 KCl, 0.88 MgCl$_2$, 1.45 CaCl$_2$, and 3.5 glucose. Subsequently, nerves were sectioned with a razor blade, and the tissue was frozen by slamming against a liquid helium–cooled copper block (E7200; Polaron) as previously reported (Gotow et al., 1999). The frozen tissue was mounted onto the freeze fracture apparatus (BAF 400D; Balzers), fractured, and then deep etched and rotary replicated with platinum/carbon at an angle of 25°. The replicates were examined with a Hitachi H-300 electron microscope at 75 kV.

Nerve conduction velocity measurements
Nerve conduction velocities were measured in the sciatic nerve, interosseus muscle system of 5-mo-old mice (Calcutt et al., 1990). In brief, mice were anesthetized with halothane (4% in O$_2$ for induction, 2–3% for maintenance), and rectal temperature was maintained at 37°C by a heating lamp and thermal pad connected to a temperature regulator and the rectal thermistor probe. The sciatic nerve was stimulated with single supramaximal square wave pulses (4–8 V and 0.05 ms duration) via fine needle electrodes placed at the sciatic notch and Achilles tendon. Evoked electromyograms were recorded from the interosseus muscles of the ipsilateral foot via two fine needle electrodes and displayed on a digital storage oscilloscope. The distance between the two sites of stimulation was measured using calipers, and conduction velocity was calculated as previously described (Calcutt et al., 1990). Measurements were made in triplicate from five animals per genotype, and the median was used as the measure of velocity. Statistical ANOVA was performed with subsequent Bonferroni multiple comparisons test post-hoc analysis using InStat.

Sciatic nerve regeneration measurements
Mice were placed under Metophane anesthesia, and the sciatic nerve was exposed via an incision in the flank followed by separation of underlying musculature by blunt dissection. The nerve is crushed using fine jewelers forceps at the level of the obturator tendon. To assess functional recovery of the injured limb, the mouse was induced to spread its toes by briefly lifting the hindlimbs off the bench. Distance from first to fifth digits was measured with a divider and expressed as a percentage of preinjury spread distance.

Activity wheels
Mice were placed in a single activity wheel chamber system (Lafayette Instruments) for 14 d. Activity was measured by the number of revolutions an animal would run during an ~12-h period. Revolutions were counted using an optical sensor that detects wheel motion and were stored on an activity wheel counter (Lafayette Instruments). Revolutions were converted into kilometers based upon a 5-inch diameter activity wheel.

References

Bartsch, U., F. Kirchhoff, and M. Schachner. 1989. Immunohistological localization of the adhesion molecules L1, N-CAM, and MAG in the developing and adult optic nerve of mice. *J. Comp. Neurol.* 284:451–462.

Calcutt, N.A., D.R. Tomlinson, and S. Biswas. 1990. Coexistence of nerve conduction deficit with increased Na(+)-K(+)-ATPase activity in galactose-fed mice. Implications for polyol pathway and diabetic neuropathy. *Diabetes.* 39:663–666.

Chen, J., T. Nakata, Z. Zhang, and N. Hirokawa. 2000. The C-terminal tail domain of neurofilament protein-H (NF-H) forms the crossbridges and regulates neurofilament bundle formation. *J. Cell Sci.* 113(Pt 21):3861–3869.

Collard, J.F., F. Cote, and J.P. Julien. 1995. Defective axonal transport in a transgenic mouse model of amyotrophic lateral sclerosis. *Nature.* 375:61–64.

Conway, J.H., and N.J.A. Sloane. 1999. Sphere packings, lattices, and groups. Springer-Verlag New York Inc., New York. 703 pp.

Cosgaya, J.M., J.R. Chan, and E.M. Shooter. 2002. The neurotrophin receptor p75NTR as a positive modulator of myelination. *Science.* 298:1245–1248.

Cote, F., J.F. Collard, and J.P. Julien. 1993. Progressive neuronopathy in transgenic mice expressing the human neurofilament heavy gene: a mouse model of amyotrophic lateral sclerosis. *Cell.* 73:35–46.

Dashiell, S.M., S.L. Tanner, H.C. Pant, and R.H. Quarles. 2002. Myelin-associated glycoprotein modulates expression and phosphorylation of neuronal cytoskeletal elements and their associated kinases. *J. Neurochem.* 81:1263–1272.

de Waegh, S.M., V.M. Lee, and S.T. Brady. 1992. Local modulation of neurofilament phosphorylation, axonal caliber, and slow axonal transport by myelinating Schwann cells. *Cell.* 68:451–463.

Elder, G.A., V.L. Friedrich, Jr., P. Bosco, C. Kang, A. Gourov, P.H. Tu, V.M. Lee, and R.A. Lazzarini. 1998. Absence of the mid-sized neurofilament subunit decreases axonal calibers, levels of light neurofilament (NF-L), and neurofilament content. *J. Cell Biol.* 141:727–739.

Eyer, J., and A. Peterson. 1994. Neurofilament-deficient axons and perikaryal aggregates in viable transgenic mice expressing a neurofilament-beta-galactosidase fusion protein. *Neuron.* 12:389–405.

Gill, S.R., P.C. Wong, M.J. Monteiro, and D.W. Cleveland. 1990. Assembly properties of dominant and recessive mutations in the small mouse neurofilament (NF-L) subunit. *J. Cell Biol.* 111:2005–2019.

Gotow, T., J.F. Leterrier, Y. Ohsawa, T. Watanabe, K. Isahara, R. Shibata, K. Ikenaka, and Y. Uchiyama. 1999. Abnormal expression of neurofilament proteins in dysmyelinating axons located in the central nervous system of jimpy mutant mice. *Eur. J. Neurosci.* 11:3893–3903.

Hirokawa, N., M.A. Glicksman, and M.B. Willard. 1984. Organization of mammalian neurofilament polypeptides within the neuronal cytoskeleton. *J. Cell Biol.* 98:1523–1536.

Hisanaga, S., and N. Hirokawa. 1988. Structure of the peripheral domains of

neurofilaments revealed by low angle rotary shadowing. *J. Mol. Biol.* 202: 297–305.

Hoffman, P.N., D.W. Cleveland, J.W. Griffin, P.W. Landes, N.J. Cowan, and D.L. Price. 1987. Neurofilament gene expression: a major determinant of axonal caliber. *Proc. Natl. Acad. Sci. USA.* 84:3472–3476.

Hsieh, S.T., G.J. Kidd, T.O. Crawford, Z. Xu, W.M. Lin, B.D. Trapp, D.W. Cleveland, and J.W. Griffin. 1994. Regional modulation of neurofilament organization by myelination in normal axons. *J. Neurosci.* 14:6392–6401.

Jacomy, H., Q. Zhu, S. Couillard-Després, J.M. Beaulieu, and J.P. Julien. 1999. Disruption of type IV intermediate filament network in mice lacking the neurofilament medium and heavy subunits. *J. Neurochem.* 73:972–984.

Julien, J.P., and W.E. Mushynski. 1982. Multiple phosphorylation sites in mammalian neurofilament polypeptides. *J. Biol. Chem.* 257:10467–10470.

Lee, M.K., J.B. Tuttle, L.I. Rebhun, D.W. Cleveland, and A. Frankfurter. 1990. The expression and posttranslational modification of a neuron-specific beta-tubulin isotype during chick embryogenesis. *Cell Motil. Cytoskeleton.* 17:118–132.

Lehmann, M., A. Fournier, I. Selles-Navarro, P. Dergham, A. Sebok, N. Leclerc, G. Tigyi, and L. McKerracher. 1999. Inactivation of Rho signaling pathway promotes CNS axon regeneration. *J. Neurosci.* 19:7537–7547.

Lopata, M.A., and D.W. Cleveland. 1987. In vivo microtubules are copolymers of available beta-tubulin isotypes: localization of each of six vertebrate beta-tubulin isotypes using polyclonal antibodies elicited by synthetic peptide antigens. *J. Cell Biol.* 105:1707–1720.

Lunn, M.P., T.O. Crawford, R.A. Hughes, J.W. Griffin, and K.A. Sheikh. 2002. Anti-myelin-associated glycoprotein antibodies alter neurofilament spacing. *Brain.* 125:904–911.

Marszalek, J.R., T.L. Williamson, M.K. Lee, Z. Xu, P.N. Hoffman, M.W. Becher, T.O. Crawford, and D.W. Cleveland. 1996. Neurofilament subunit NF-H modulates axonal diameter by selectively slowing neurofilament transport. *J. Cell Biol.* 135:711–724.

Mirsky, R., K.R. Jessen, A. Brennan, D. Parkinson, Z. Dong, C. Meier, E. Parmantier, and D. Lawson. 2002. Schwann cells as regulators of nerve development. *J. Physiol. (Paris).* 96:17–24.

Monteiro, M.J., P.N. Hoffman, J.D. Gearhart, and D.W. Cleveland. 1990. Expression of NF-L in both neuronal and nonneuronal cells of transgenic mice: increased neurofilament density in axons without affecting caliber. *J. Cell Biol.* 111:1543–1557.

Nakagawa, T., J. Chen, Z. Zhang, Y. Kanai, and N. Hirokawa. 1995. Two distinct functions of the carboxyl-terminal tail domain of NF-M upon neurofilament assembly: cross-bridge formation and longitudinal elongation of filaments. *J. Cell Biol.* 129:411–429.

Niederost, B., T. Oertle, J. Fritsche, R.A. McKinney, and C.E. Bandtlow. 2002. Nogo-A and myelin-associated glycoprotein mediate neurite growth inhibition by antagonistic regulation of RhoA and Rac1. *J. Neurosci.* 22:10368–10376.

Nikolic, M., M.M. Chou, W. Lu, B.J. Mayer, and L.H. Tsai. 1998. The p35/Cdk5 kinase is a neuron-specific Rac effector that inhibits Pak1 activity. *Nature.* 395:194–198.

Ohara, O., Y. Gahara, T. Miyake, H. Teraoka, and T. Kitamura. 1993. Neurofilament deficiency in quail caused by nonsense mutation in neurofilament-L gene. *J. Cell Biol.* 121:387–395.

Pant, A.C., Veeranna, H.C. Pant, and N. Amin. 1997. Phosphorylation of human high molecular weight neurofilament protein (hNF-H) by neuronal cyclin-dependent kinase 5 (cdk5). *Brain Res.* 765:259–266.

Rao, M.V., M.K. Houseweart, T.L. Williamson, T.O. Crawford, J. Folmer, and D.W. Cleveland. 1998. Neurofilament-dependent radial growth of motor axons and axonal organization of neurofilaments does not require the neurofilament heavy subunit (NF-H) or its phosphorylation. *J. Cell Biol.* 143:171–181.

Rao, M.V., M.L. Garcia, Y. Miyazaki, T. Gotow, A. Yaun, S. Mattina, C.M. Ward, N.A. Calcutt, Y. Uchiyama, R.A. Nixon, and D.W. Cleveland. 2002. Gene replacement in mice reveals that the heavily phosphorylated tail of neurofilament heavy subunit does not affect axonal caliber or the transit of cargoes in slow axonal transport. *J. Cell Biol.* 158:681–693.

Salehi, A.H., P.P. Roux, C.J. Kubu, C. Zeindler, A. Bhakar, L.L. Tannis, J.M. Verdi, and P.A. Barker. 2000. NRAGE, a novel MAGE protein, interacts with the p75 neurotrophin receptor and facilitates nerve growth factor-

dependent apoptosis. *Neuron.* 27:279–288.

Shetty, K.T., W.T. Link, and H.C. Pant. 1993. cdc2-like kinase from rat spinal cord specifically phosphorylates KSPXK motifs in neurofilament proteins: isolation and characterization. *Proc. Natl. Acad. Sci. USA.* 90:6844–6848.

Shetty, K.T., S. Kaech, W.T. Link, H. Jaffe, C.M. Flores, S. Wray, H.C. Pant, and S. Beushausen. 1995. Molecular characterization of a neuronal-specific protein that stimulates the activity of Cdk5. *J. Neurochem.* 64:1988–1995.

Svitkina, T.M., A.B. Verkhovsky, and G.G. Borisy. 1996. Plectin sidearms mediate interaction of intermediate filaments with microtubules and other components of the cytoskeleton. *J. Cell Biol.* 135:991–1007.

Tcherpakov, M., F.C. Bronfman, S.G. Conticello, A. Vaskovsky, Z. Levy, M. Niinobe, K. Yoshikawa, E. Arenas, and M. Fainzilber. 2002. The p75 neurotrophin receptor interacts with multiple MAGE proteins. *J. Biol. Chem.* 277: 49101–49104.

Trapp, B.D., S.B. Andrews, C. Cootauco, and R. Quarles. 1989. The myelin-associated glycoprotein is enriched in multivesicular bodies and periaxonal membranes of actively myelinating oligodendrocytes. *J. Cell Biol.* 109:2417–2426.

Tu, P.H., G. Elder, R.A. Lazzarini, D. Nelson, J.Q. Trojanowski, and V.M. Lee. 1995. Overexpression of the human NFM subunit in transgenic mice modifies the level of endogenous NFL and the phosphorylation state of NFH subunits. *J. Cell Biol.* 129:1629–1640.

Veeranna, N.D. Amin, N.G. Ahn, H. Jaffe, C.A. Winters, P. Grant, and H.C. Pant. 1998. Mitogen-activated protein kinases (Erk1,2) phosphorylate Lys-Ser-Pro (KSP) repeats in neurofilament proteins NF-H and NF-M. *J. Neurosci.* 18:4008–4021.

Vyas, A.A., H.V. Patel, S.E. Fromholt, M. Heffer-Lauc, K.A. Vyas, J. Dang, M. Schachner, and R.L. Schnaar. 2002. Gangliosides are functional nerve cell ligands for myelin-associated glycoprotein (MAG), an inhibitor of nerve regeneration. *Proc. Natl. Acad. Sci. USA.* 99:8412–8417.

Wang, K.C., J.A. Kim, R. Sivasankaran, R. Segal, and Z. He. 2002. P75 interacts with the Nogo receptor as a co-receptor for Nogo, MAG and OMgp. *Nature.* 420:74–78.

Wiche, G. 1989. Plectin: general overview and appraisal of its potential role as a subunit protein of the cytomatrix. *Crit. Rev. Biochem. Mol. Biol.* 24:41–67.

Wiche, G. 1998. Role of plectin in cytoskeleton organization and dynamics. *J. Cell Sci.* 111:2477–2486.

Wong, P.C., J. Marszalek, T.O. Crawford, Z. Xu, S.T. Hsieh, J.W. Griffin, and D.W. Cleveland. 1995. Increasing neurofilament subunit NF-M expression reduces axonal NF-H, inhibits radial growth, and results in neurofilamentous accumulation in motor neurons. *J. Cell Biol.* 130:1413–1422.

Wong, S.T., J.R. Henley, K.C. Kanning, K.H. Huang, M. Bothwell, and M.M. Poo. 2002. A p75(NTR) and Nogo receptor complex mediates repulsive signaling by myelin-associated glycoprotein. *Nat. Neurosci.* 5:1302–1308.

Xu, Z., L.C. Cork, J.W. Griffin, and D.W. Cleveland. 1993. Increased expression of neurofilament subunit NF-L produces morphological alterations that resemble the pathology of human motor neuron disease. *Cell.* 73:23–33.

Xu, Z., J.R. Marszalek, M.K. Lee, P.C. Wong, J. Folmer, T.O. Crawford, S.T. Hsieh, J.W. Griffin, and D.W. Cleveland. 1996. Subunit composition of neurofilaments specifies axonal diameter. *J. Cell Biol.* 133:1061–1069.

Xu, Z.S., W.S. Liu, and M.B. Willard. 1992. Identification of six phosphorylation sites in the COOH-terminal tail region of the rat neurofilament protein M. *J. Biol. Chem.* 267:4467–4471.

Yamashita, T., H. Higuchi, and M. Tohyama. 2002. The p75 receptor transduces the signal from myelin-associated glycoprotein to Rho. *J. Cell Biol.* 157:565–570.

Yang, L.J., C.B. Zeller, N.L. Shaper, M. Kiso, A. Hasegawa, R.E. Shapiro, and R.L. Schnaar. 1996a. Gangliosides are neuronal ligands for myelin-associated glycoprotein. *Proc. Natl. Acad. Sci. USA.* 93:814–818.

Yang, Y., J. Dowling, Q.C. Yu, P. Kouklis, D.W. Cleveland, and E. Fuchs. 1996b. An essential cytoskeletal linker protein connecting actin microfilaments to intermediate filaments. *Cell.* 86:655–665.

Yin, X., T.O. Crawford, J.W. Griffin, P. Tu, V.M. Lee, C. Li, J. Roder, and B.D. Trapp. 1998. Myelin-associated glycoprotein is a myelin signal that modulates the caliber of myelinated axons. *J. Neurosci.* 18:1953–1962.

Zhu, Q., S. Couillard-Després, and J.P. Julien. 1997. Delayed maturation of regenerating myelinated axons in mice lacking neurofilaments. *Exp. Neurol.* 148:299–316.